atmosphere

Article

Retrieval of Aerosol Optical Depth and FMF over East Asia from Directional Intensity and Polarization Measurements of PARASOL

Shupeng Wang [1,2], Li Fang [3,*], Weishu Gong [4], Weihe Wang [1,2] and Shihao Tang [1,2]

1 Key Laboratory of Radiometric Calibration and Validation for Environmental Satellites, China Meteorological Administration, Beijing 100081, China
2 Innovation Center for FengYun Meteorological Satellite (FYSIC), Beijing 100081, China
3 China Siwei Surveying and Mapping Technology Co., Ltd., Beijing 100094, China
4 Department of Geographical Sciences, University of Maryland, 2181 Samuel J. LeFrak Hall, 7251 Preinkert Drive, College Park, MD 20742, USA
* Correspondence: fangli@chinasiwei.com

Abstract: The advantages of performing aerosol retrieval with multi-angle, multi-spectral photopolarimetric measurements over intensity-only measurements come from this technique's sensitivity to aerosols' microphysical properties, such as their particle size, shape, and complex refraction index. In this study, an extended LUT (Look Up Table) algorithm inherited from a previous work based on the assumption of surface reflectance spectral shape invariance is proposed and applied to PARASOL (Polarization and Anisotropy of Reflectances for Atmospheric Science coupled with Observations from a Lidar) measurements to retrieve aerosols' optical properties including aerosol optical depth (AOD) and aerosol fine-mode fraction (FMF). Case studies conducted over East China for different aerosol scenes are investigated. A comparison between the retrieved AOD regional distribution and the corresponding MODIS (Moderate-resolution Imaging Spectroradiometer) C6 AOD products shows similar spatial distributions in the Jing-Jin-Ji (Beijing–Tianjin–Hebei, China's mega city cluster) region. The PARASOL AOD retrievals were compared against the AOD measurements of seven AERONET (Aerosol Robotic Network) stations in China to evaluate the performance of the retrieval algorithm. In the fine-particle-dominated regions, lower RMSEs were found at Beijing and Hefei urban stations (0.16 and 0.18, respectively) compared to those at other fine-particle-dominated AERONET stations, which can be attributed to the assumption of surface reflectance spectral shape invariance that has significant advantages in separating the contribution of surface and aerosol scattering in urban areas. For the FMF validation, an RMSE of 0.23, a correlation of 0.57, and a bias of −0.01 were found. These results show that the algorithm performs reasonably in distinguishing the contribution of fine and coarse particles.

Keywords: polarization; AOD; FMF; aerosol retrieval; POLDER

check for updates

Citation: Wang, S.; Fang, L.; Gong, W.; Wang, W.; Tang, S. Retrieval of Aerosol Optical Depth and FMF over East Asia from Directional Intensity and Polarization Measurements of PARASOL. *Atmosphere* **2024**, *15*, 6. https://doi.org/10.3390/atmos15010006

Academic Editors: Chang H. Jung, Jingsha Xu, Lei Liu, Shanshan Tang and Alexandros Papayannis

Received: 22 August 2023
Revised: 1 December 2023
Accepted: 18 December 2023
Published: 20 December 2023

1. Introduction

Being influenced by both natural phenomena and human activities, atmospheric aerosol distributions are complex, with urban areas in particular being dominated by anthropogenic aerosols that are released from diesel-powered vehicles and industrial activity [1,2]. Increased emissions of aerosol particles associated with economic growth can lead to increased emissions of hazardous air pollutants. Fine particles increase the mortality rates of patients suffering from heart and/or lung diseases because fine particles can penetrate deeper into the lungs than coarser inhalable particles and so have a more severe impact on public health [3]. Alongside fine particles causing air pollution, better estimates of the perturbations of earth's radiation budget require accurate optical and physical parameters of both fine and coarse particles such as aerosol optical depth, single-scattering albedo, and size distribution [4]. Daily measurement of these aerosol properties globally can only be achieved using satellite remote sensing.

Aerosol retrieval using multi-angle, multi-spectral photopolarimetric measurements has higher sensitivity to the microphysical properties of aerosols, such as their particle size, shape, and complex refraction index, compared with using intensity-only measurements alone [4,5]. PARASOL provided multi-spectral, multi-angle, and photopolarimetric measurements of intensity and polarization with a swath of 1600 km cross track [6]. The Directional Polarimetric Camera (DPC) was mounted on the Gaofen-5 (GF-5) satellite in orbit between May 2018 and April 2020. It is the first Chinese MAP (Multi-Angle Polarimeter) capable of aerosol and cloud retrieval. The DPC performed multi-directional measurements in eight spectral channels from 443 nm to 910 nm. It also provided polarization measurements in three channels of 490 nm, 670 nm, and 865 nm. It measures at up to 12 angles [7–9].

Different aerosol retrieval algorithms based on the LUT construction introduce both intensity and polarization measurements for total AOD retrieval [5,10]. The main difference between these algorithms stems from the selection of a semi-empirical surface reflectance model and proper aerosol models that characterize the aerosol properties over the region of interest. There are also aerosol retrieval algorithms that use the data redundancy available from multi-spectral, multi-directional, and polarized measurements such as the GRASP (Generalized Retrieval of Aerosol and Surface Properties) algorithm [11,12], the SRON (Netherlands Institute for Space Research) algorithm [13–16], and the algorithm for AirMSPI (Airborne Multi-angle SpectroPolarimeter Imager) [17]. These algorithms fit MAP observations that include both measurements of radiance and linear polarization in selected spectral channels and viewing geometries simultaneously [18]. They do not rely entirely on LUT. Some of them use LUT to obtain a first guess and are designed for the retrieval of an extended set of aerosol microphysical parameters for both fine and coarse particles.

In this study, an extended LUT aerosol retrieval algorithm based on the assumption of surface reflectance spectral shape invariance [19] was applied to PARASOL measurements to retrieve aerosol properties. The retrieved parameters include the aerosol total AOD and FMF (fine-mode fraction) that relate to aerosols' microphysical properties. Section 2 presents the detailed retrieval approach, the determination of the aerosol model's parameters, and the data-processing flow. The regional retrieval for haze, clear sky, and dust cases in the Jing-Jin-Ji region (Beijing–Tianjin–Hebei, one of China's mega city clusters) and a comparison with the MODIS AOD products are presented in Section 3. Based on ground-based data from Aerosol Robotic Network (AERONET) sites in China [20,21], a validation of the retrieval results obtained using our method is also presented in Section 3. The conclusions are given in Section 4.

2. Methodology

Similar to the algorithm described in Wang et al.'s study from 2015 [19], the spectral reflectance angular shape similarity principle was employed to separate the TOA (Top Of Atmosphere) reflectance contribution from aerosol scattering and surface reflectance instead of using a semi-empirical surface reflectance model.

Figure 1 shows the aerosol retrieval flow. The AODs and aerosol modes with the Xangular index (detailed in Section 2.1) within the threshold can be considered preliminary aerosol retrieval results. Preliminary aerosol retrievals with similar Xangular indexes represent similar aerosol properties, which can be distinguished using polarized measurements in the second step. Different aerosol components were combined to form different aerosol modes in the LUT construction described in Section 2.2.

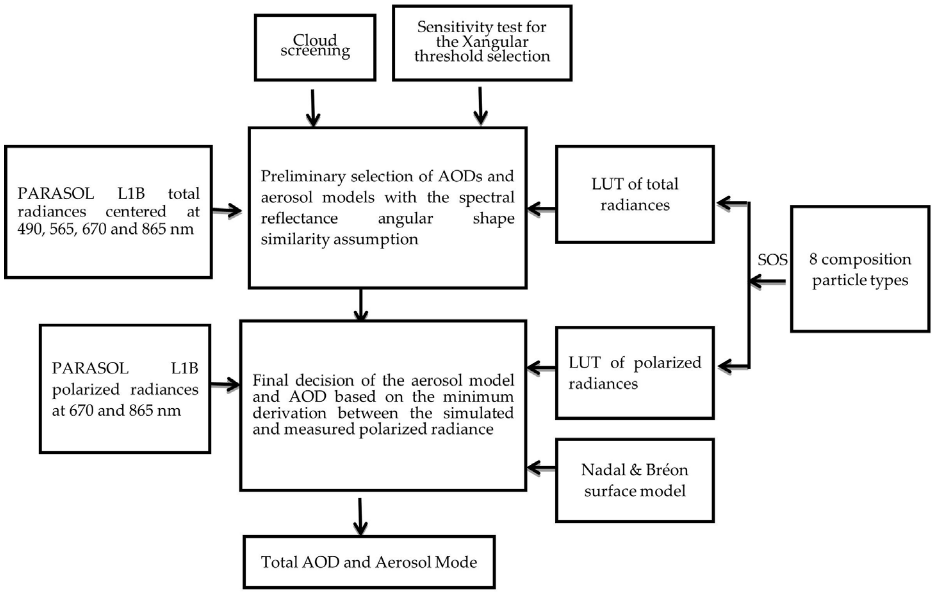

Figure 1. A flowchart of the aerosol retrieval process.

The vector radiative transfer forward model of SOS (Successive Orders of Scattering) [22] was used to simulate the TOA intensity and polarized measurements in PARASOL spectral bands to build the LUT. Only the pixels filtered by the cloud mask of PARASOL were used for retrieval [23,24].

2.1. Retrieval Algorithm

The surface spectral reflectance angular shape invariance principle suggests that the angular shape of the surface hemispherical–directional reflectance factor (HDRF) can be expected to be nearly invariant in the visible and shortwave infrared (SWIR) spectral regions. This is because the scale of the macroscopic structure of the underlying surface is much larger than the wavelengths of the incident light [25]. The sensitivity of the similarity of HDRF shapes has been tested for PARASOL measurements over areas of high and relatively low surface heterogeneity [19]. Although there is strong spectral variation in surface reflectance, it shows the angular shapes of the HDRFs are independent of the wavelength at the spatial resolution of PARASOL nadir pixels, indicating the reliability of the assumption.

In the retrieval, the HDRF of the PARASOL nadir pixel needs to be calculated using

$$\rho_\lambda(\mu_s, -\mu_v, \Delta\phi) = \frac{L_\lambda^{meas}(\mu_s, -\mu_v, \Delta\phi) - L_\lambda^{atm}(\mu_s, -\mu_v, \Delta\phi)}{\left[exp(-\tau_\lambda/\mu_v) + t_\lambda^{diff}(-\mu_v)\right] \times L_\lambda^{surf}(\mu_s)} \quad (1)$$

where ρ_λ is the surface HDRF at wavelength λ; $\mu_s, -\mu_v, \Delta\phi$ represent the cosine of the view zenith angle, the cosine of the solar zenith angle, and the relative azimuth angle, respectively; L_λ^{meas} denotes the TOA radiance measurements; L_λ^{atm} is the atmospheric path radiance; τ_λ is the total atmospheric optical depth; t_λ^{diff} is the upward atmospheric diffuse transmittance; and L_λ^{surf} is the downwelling normalized illumination at the surface level.

Via dividing ρ_λ by the angular average value $\langle\rho_\lambda\rangle_{dir}$, this normalized HDRF, $\rho_{dirnorm,\lambda}$ is yielded as follows:

$$\rho_{dirnorm,\lambda}(i) = \frac{\rho_\lambda(i)}{\langle\rho_\lambda(i)\rangle_{dir}} = \frac{\left[L_\lambda^{meas}(i) - L_\lambda^{atm}(i)\right] / \left[exp(-\tau_\lambda/\mu_i) + t_\lambda^{diff}(i)\right]}{\left\langle \left[L_\lambda^{meas} - L_\lambda^{atm}\right] / \left[exp(-\tau_\lambda/\mu) + t_\lambda^{diff}\right] \right\rangle_{dir}} \quad (2)$$

where $\mu_s, -\mu_v, \Delta\phi$, are represented using the angular index i. For the normalized HDRF that will be used in Equation (3) to calculate the spectral reflectance shape invariance index X^2_{angular}, the atmospheric parameters in Equation (2) are pre-simulated using the SOS vector radiative transfer model for the pre-determined aerosol models [22].

If the correct aerosol optical depth and aerosol model are selected, $\rho_{dirnorm,\lambda}$ will be wavelength-independent. An overall residual as a function of aerosol model and AOD is defined as

$$X^2_{\text{angular}}(\tau_a,\ \text{model}) = \frac{\sum_\lambda w_\lambda \sum_i q_i \left[\rho_{dirnorm,\lambda}(i) - \langle\rho_{dirnorm}(i)\rangle_\lambda\right]^2}{(0.05)^2 \sum_\lambda w_\lambda \sum_i q_i} \tag{3}$$

where w_λ are the band weights,$\langle\rho_{dirnorm}\rangle_\lambda$ is the spectral average of $\rho_{dirnorm,\lambda}$, and q_i denotes the angular weights. Considering the departures from the common angular shape at the shorter wavelengths are more heavily penalized, the w_λ values of 4, 3, 2, and 1 are assigned to the 4 bands of blue, green, red, and near-IR, respectively. The angular weights, denoted by q_i, are set to $1/\mu_v$, which suggests higher atmospheric sensitivity under oblique views. The retrieval algorithm based on the surface reflectance angular shape similarity derives from the AlongTrack Scanning Radiometer (ATSR)-2 and the Multi-angle Imaging SpectroRadiometer (MISR) aerosol retrieval equipment. MISR aerosol retrieval uses four bands of blue, green, red, and near-IR, and the inclusion of the other two bands of PARASOL may affect the applicability of the assumption.

In the retrieval process, a proper threshold for Xangular is selected to determine which preliminary aerosol models to use and the corresponding AODs that satisfy the assumption of the spectral reflectance shape invariance principle. The threshold mainly depends on the similarity of the surface reflectance spectral variance to the spectral variance of atmospheric scattering. Underlying surfaces with greater surface heterogeneity, such as urban areas, show obviously different spectral variance compared with that of atmospheric scattering, leading to a smaller threshold.

The threshold in this work was determined based on a sensitivity study reported in [19]. In the case of POLDER spatial resolution, a threshold of 2 for Xangular was considered to guarantee that the assumption was effective. A much wider range of sensitivity tests was carried out; moreover, in order to increase the range of the preliminary inversion results in the first step, the threshold of 5 is used in this work to ensure wider applicability of the assumption and the accuracy of aerosol inversion in East Asia.

For the preliminary aerosol models and AODs achieved in the first step, the corresponding multi-angle polarized reflectances at 670 nm and 865 nm can be obtained using the polarized LUT. Similar to the previously operational land aerosol inversion approach of POLDER/PARASOL [10], the minimum derivation between the simulated and measured polarized radiance leads to the final determination of the aerosol parameters. The FMF can be determined from the parameters of the retrieved aerosol model.

In addition, in order to avoid large AOD retrieval bias caused by the depolarization effect of a high coarse particle loading, the preliminary retrievals with a predominantly aerosol mode of coarse particles and AOD >1.5 were excluded. Although this setting eliminates the possibility of aerosol retrieval under the cases of high coarse particle loadings, it improves the effectiveness and robustness of the algorithm.

2.2. Aerosol Models and the Construction of LUT

In the previous work described in [19], regional average aerosol model parameters obtained from 5 years' worth of data from AERONET site were used for LUT construction and retrieval. Compared with the previous paper, this work updates the more detailed aerosol modes that are similar to MISR operational retrieval version 23. Eight aerosol components of the aerosol mode database were selected and combined to generate 46 different aerosol mixtures suitable for global retrieval.

The aerosol models selected for LUT construction are similar to those used in the MISR operational Version 23 retrieval process, as described in the Aerosol Climatology

Product (ACP), which is composed of two parts, an Aerosol Physical and Optical Properties (APOP) file and a tropospheric Aerosol Mixture file [26]. The APOP file contains detailed information on the microphysical and scattering characteristics of 21 different single-composition aerosol particle types, of which 8 were used in the retrieval process (see Table 1). During the retrieval process, 46 distinct aerosol models were created as mixtures of these components with a specific ratio using information detailed in the Aerosol Mixture file of the ACP (see Table 2). The algorithm is based on a bimodal description of aerosols in fine and coarse modes. Both the fine and coarse modes are described by a lognormal size distribution. For fine-mode particles, a spherical particle assumption was used, and the optical properties were simulated using MIE theory [27]. For coarse-mode particles, in order to account for aerosol non-sphericity, the numerical tool for the fast calculation of the scattering properties of a spheroid mixture was used [28].

Table 1. Aerosol components.

Aerosol Type	r_m (μm)	σ	Real Refractive Index	Imaginary Refractive Index	Effective Radius (μm)	Single Scattering Albedo
1: spherical	0.03	0.501	1.45	0.00	0.06	1.0
2: spherical	0.06	0.531	1.45	0.00	0.12	1.0
3: spherical	0.12	0.560	1.45	0.00	0.26	1.0
6: spherical	1.0	0.642	1.45	0.00	2.80	1.0
8: spherical	0.06	0.531	1.45	0.0147	0.12	B:0.911 G:0.900 R: 0.855 N: 0.853
14: spherical	0.06	0.531	1.45	0.0325	0.12	B:0.821 G:0.800 R: 0.773 N: 0.720
19: dust	0.5	0.405	B:1.50 G:1.51 R:1.51 N:1.51	B:0.0041 G:0.0021 R:0.00065 N:0.00047	0.21	B:0.919 G:0.977 R: 0.994 N: 0.997
21: dust	1.0	0.693	1.51	B:0.0041 G:0.0021 R:0.00065 N:0.00047	3.32	B:0.810 G:0.902 R: 0.971 N: 0.983

B = blue, G = green, R = red, and N = near-IR.

Table 2. PARASOL retrieval aerosol mixtures.

Model Number	Components	Mixture Fractional Optical Depth (Green Band)
1–5: bimodal	1 and 6	Range: 1.0 (1) and 0.0 (6) to 0.2 (1) and 0.8 (6)
6–10: bimodal	2 and 6	Range: 1.0 (2) and 0.0 (6) to 0.2 (2) and 0.8 (6)
11–15: bimodal	3 and 6	Range: 1.0 (3) and 0.0 (6) to 0.2 (3) and 0.8 (6)
16–20: bimodal	8 and 6	Range: 1.0 (8) and 0.0 (6) to 0.2 (8) and 0.8 (6)
21–25: bimodal	14 and 6	Range: 1.0 (14) and 0.0 (6) to 0.2 (14) and 0.8 (6)
26–28: trimodal	2, 6, and 19	Range: 0.72 (2), 0.08 (6), and 0.2 (19) to 0.16 (2), 0.64 (6), and 0.2 (19)
29–31: trimodal	2, 6, and 19	Range: 0.54 (2), 0.06 (6), and 0.4 (19) to 0.12 (2), 0.48 (6), and 0.4 (19)
32–34: trimodal	2, 6, and 19	Range: 0.36 (2), 0.04 (6), and 0.6 (19) to 0.08 (2), 0.32 (6), and 0.6 (19)
35–37: trimodal	2, 6, and 19	Range: 0.18 (2), 0.02 (6), and 0.8 (19) to 0.04 (2), 0.16 (6), and 0.8 (19)
38–40: trimodal	2, 19, and 21	Range: 0.4 (2), 0.48 (19), and 0.12 (21) to 0.4 (2), 0.12 (19), and 0.48 (21)
41–43: trimodal	2, 19, and 21	Range: 0.2 (2), 0.64 (19), and 0.16 (21) to 0.2 (2), 0.16 (19), and 0.64 (21)
44–46: bimodal	19 and 21	Range: 0.8 (19) and 0.2 (21) to 0.2 (19), 9, and 0.8 (21)

Then, two LUTs need to be constructed using the SOS vector radiative transfer forward model. One is the LUT of radiance for the preliminary selection of AOD and aerosol mode.

It includes the atmospheric path radiance and the upward diffuse, azimuthally integrated atmospheric transmittance at PARASOL's spectral bands centered at 490 nm, 670 nm, and 865 nm for different AODs; different aerosol modes; and all the viewing geometry grids. The other one is the LUT of polarization for the final decision of the aerosol properties. It includes the polarized reflectance at 670 nm and 865 nm for the same aerosol property and viewing geometry settings. As the preliminary aerosol property selection uses the assumption of the spectral reflectance shape invariance principle instead of a surface reflectance model, the radiance LUT does not need to consider the contribution of surface reflectance. The polarized LUT uses the Nadal–Bréon model to simulate the surface-polarized reflectance for different surface types based on Normalized Difference Vegetation Index (NDVI) classification [29].

3. Validation and Case Studies

3.1. Validation against AERONET

For the ground-based validation, we used Level 2 AERONET data that were cloud-screened and quality-assured [30]. All one-year measurements in 2008 were collected from the seven selected AERONET sites given in Table 3. These AERONET sites cover different types of land cover and aerosol models. The annual average 440–870 nm Angstrom Exponent (AE) values obtained from the AERONET measurements in 2008 are also shown in Table 3. We extracted data between 13:00 p.m. and 14:00 p.m. local time to provide a 60 min window centered on the PARASOL overpass time of ~13:30 p.m. The AERONET sun-direct AOD measurements and FMF inverted from almucantar measurements [31] over this 60 min window were averaged for comparison with the PARASOL retrievals. The Gfrac is also given to show the fraction of good retrievals, which represent the retrievals for which the deviation from the validation data is less than $\Delta\tau = 0.05 + 0.15 \times \tau_{\mathrm{AERONET}}$, where τ is aerosol optical depth.

Table 3. Summary of the validation results for the 7 selected AERONET sites.

	Site	Average AOD	AE	Correlation	RMSE	Slope	Intercept	N *	Latitude (N)	Longitude (E)
1	Beijing	0.59	1.182	0.87	0.160	0.86	0.11	25	39.977	116.381
2	Hefei	0.48	1.137	0.49	0.182	0.95	0.12	17	31.905	117.162
3	Jingtai	0.40	0.414	0.55	0.131	0.50	0.13	17	37.333	104.1
4	SACOL	0.29	0.798	0.55	0.131	0.50	0.13	33	35.946	104.137
5	Taihu	0.61	1.214	0.69	0.327	0.96	0.10	32	31.421	120.215
6	Xianghe	0.45	1.217	0.84	0.218	0.87	0.10	47	39.75	116.953
7	Xinglong	0.18	1.200	0.58	0.206	0.74	0.15	43	40.417	117.58

* Number of samples.

Figure 2 shows the AOD validation results of all the samples. Figure 3 shows a comparison of the PARASOL AOD retrievals against the AOD measurements for each AERONET site. The aerosol models of the SACOL and Jingtai sites are coarse-particle-dominated, while the aerosol models of other sites are fine-particle-dominated. The SACOL and Jingtai sites are regarded as dust sites. Figure 2 shows a correlation coefficient of 0.645, an RMSE of 0.214, and a Gfrac of 40.4%. The fitting slopes for nearly all sites are larger than 0.7 except for those for SACOL and Jingtai. However, only the Gfrac values of SACOL and Jingtai are greater than 50%. The obviously lower slope at SACOL and Jingtai can be attributed to the exclusion of the preliminary retrievals with AOD > 1.5.

In Beijing and Hefei, the Gfrac values are greater than 40%, while those of other sites are lower than 40%. The relatively lower RMSEs in Beijing and Hefei also indicate better AOD retrieval performance as compared with other fine-particle-dominated areas. This result can be attributed to the better performance regarding the spectral reflectance shape invariance principle in urban areas with higher surface heterogeneity.

Relatively higher RMSEs of 0.218 and 0.206 were found in Xinglong and Xianghe, respectively. These two sites are located in suburban areas; here, the surface homogeneity is better than that in urban areas, so it is not helpful to use this hypothesis to distinguish between surface and atmospheric scattering contributions. In addition, the Xinglong area is mountainous, constituting an area where the topography may also lead to difficulty in separating surface and atmospheric scattering.

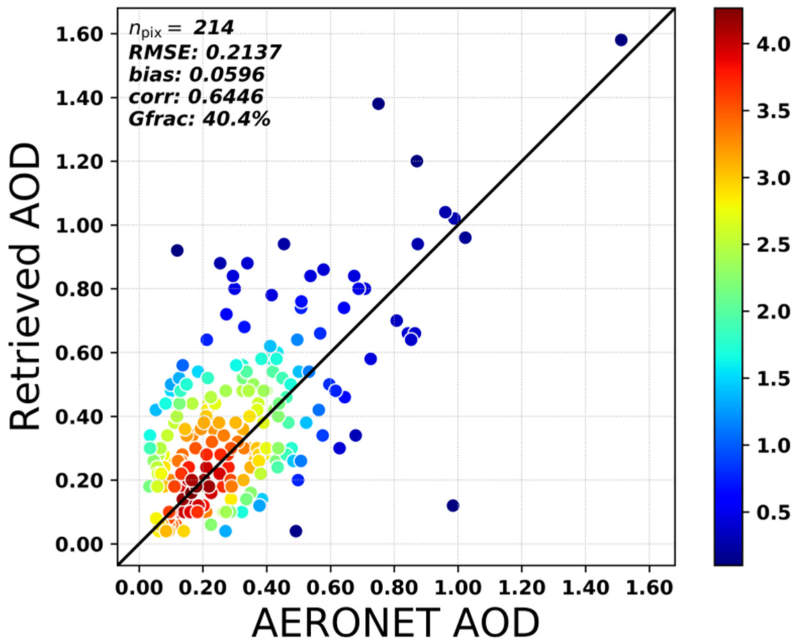

Figure 2. The AOD retrieval validation for all the samples from the 7 selected AERONET sites. The color of each point represents the density of the area where the point is located.

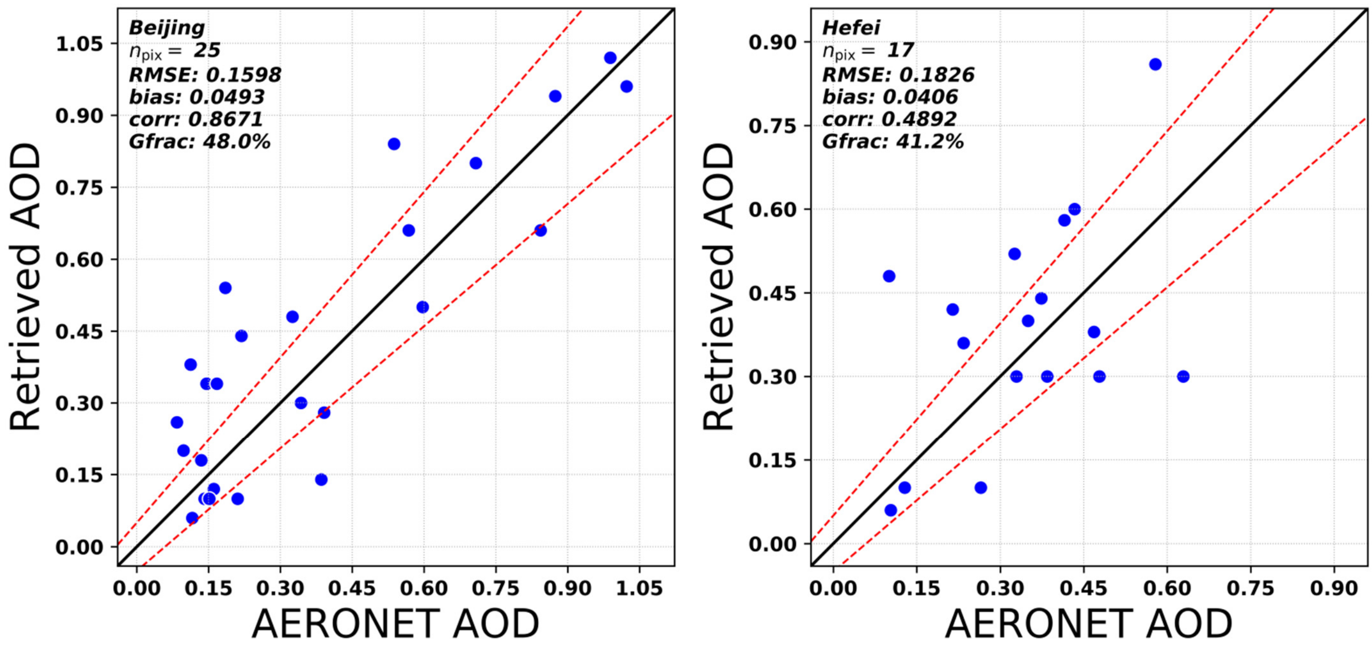

(**a**) (**b**)

Figure 3. *Cont.*

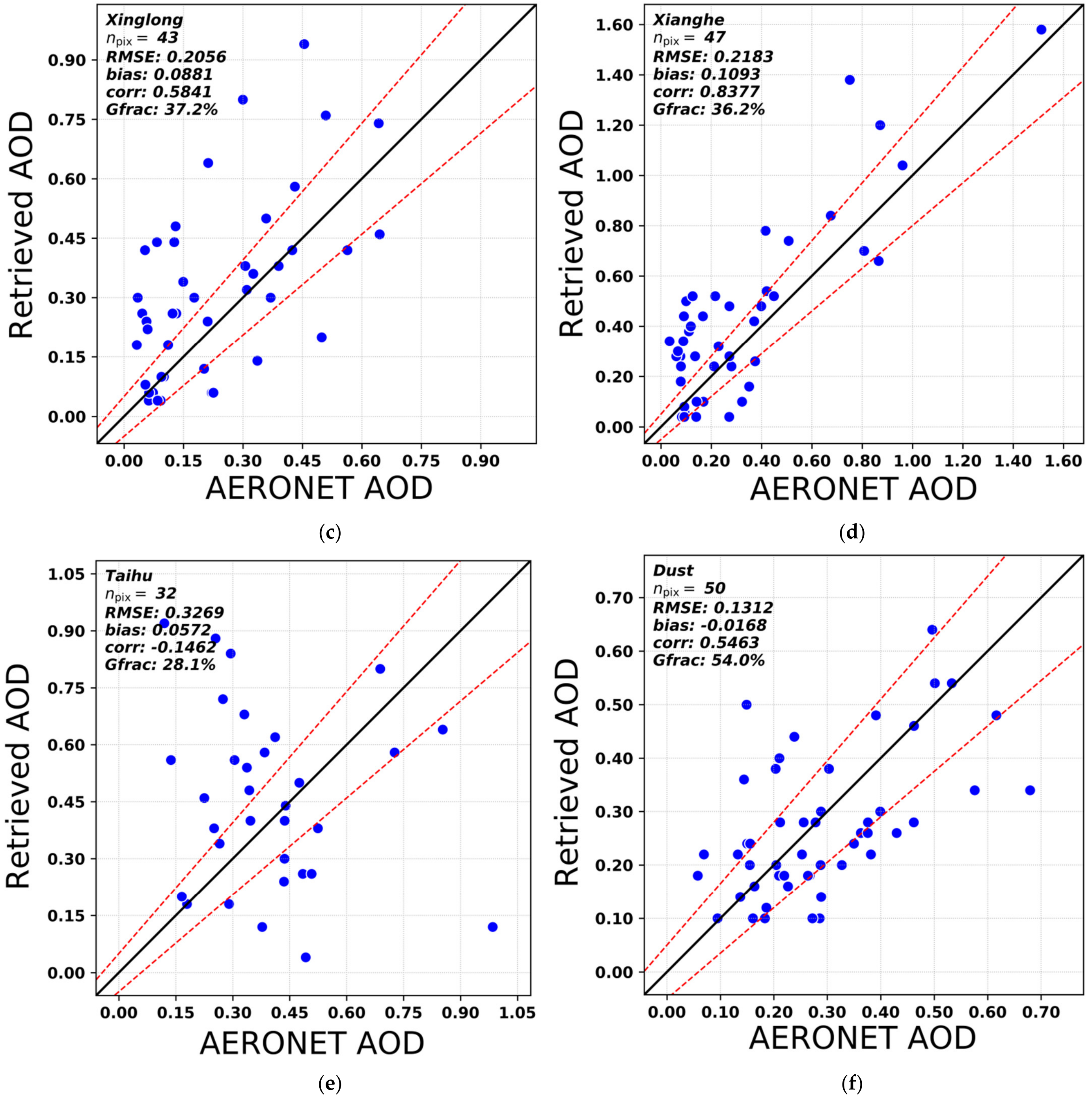

Figure 3. AOD validation for different AERONET sites of (**a**) Beijing, (**b**) Hefei, (**c**) Xinglong, (**d**) Xianghe, (**e**) Taihu and (**f**) two dust sites of Jingtai and SASOL combined.

The largest RMSE of 0.327 was found at the Taihu site. This could be due to the relatively low spatial resolution of PARASOL that probably resulted in pixels mixed with both land and water, as the site is close to Taihu Lake, measuring 2445 km^2. Since the surface reflectance angular shape similarity was used to separate the TOA reflectance contribution from aerosol scattering and the land surface reflectance, the retrieval uncertainty can be attributed to the uncertainty of the surface reflectance modeling of the land–water mixture.

Compared with the RMSE (0.228) of the AOD validation results in dusty sites reported by Fang et al. in 2022 [15], the RMSE here is much lower (0.131). On the one hand, as there is no high AOD scene from the matched AERONET validation data, the preliminary aerosol retrievals corresponding to high coarse particle loadings were excluded in the first retrieval step. In the area dominated by fine particles, the RMSE in this work (~0.24) is obviously greater than that obtained by Fang et al. in 2022, who used an optimization algorithm to process DPC data (0.151). For all the validation samples in this work, the RMSE is 0.214, which is obviously larger than the RMSE of 0.16 reported in [15]. The optimized algorithms show higher robustness and stability than LUT algorithms.

For the evaluation of the sensitivity to aerosol mode, the FMF retrievals from PARASOL were also validated. Figure 4a shows the FMF retrievals compared with the FMF retrievals of all the AERONET sites above. An RMSE of 0.23, a correlation coefficient of 0.57, and a bias of −0.01 were found. This result shows reasonable performance in distinguishing fine- and coarse-particle dominated areas from the aerosol retrieval.

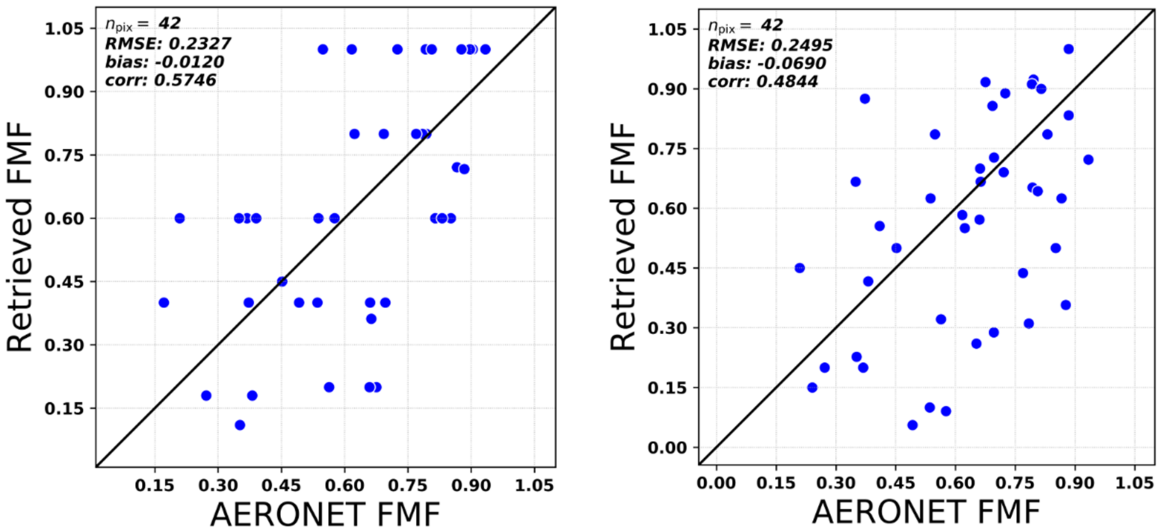

(**a**) (**b**)

Figure 4. FMF validation against AERONET retrievals for all the samples from 7 selected AERONET sites. (**a**) FMF retrieved with our algorithm, (**b**) FMF derived as the ratio of the fine AOD obtained from polarization measurements to the total AOD retrievals.

The discontinuity of the FMF retrievals can be attributed to the discontinuity of the aerosol modes pre-assumed in the LUT construction. It is also one of the main differences between the LUT algorithms and the optimized algorithms, in which the aerosol model parameters can be adjusted continuously during the inversion process and the distribution of the parameters can cover the entire parameter space. In order to avoid the discontinuity of the FMF retrievals to some extent, the fine-mode AOD data derived from polarization measurements using the algorithm proposed by Deuzé et al. (2001) [10] were used. Then, the FMF could be derived as the ratio of the fine AOD to the total AOD retrievals in this work. All the samples shown in Figure 4a were reprocessed and compared with the AERONET data, as shown in Figure 4b. The results show an RMSE of 0.25, a correlation coefficient of 0.49, and a bias of 0.06. Compared with the validation results shown in Figure 5a, relatively larger biases and lower correlations were found, which can be attributed to the additional errors brought by the fine AOD retrievals.

However, the obviously lower correlation (~0.3) for SSA validation shows the algorithm has low sensitivity to SSA. Optimized algorithms perform better for SSA retrieval, as Chen et al. (2020) found a correlation of greater than 0.5 provided by a GRASP/High-Precision and GRASP/Optimized algorithm [32]. The low sensitivity to SSA can be attributed to the fact that the algorithm based on LUT cannot search the entire aerosol mode parameter space, which is the main advantage of the optimized algorithms. Compared to the accurate aerosol mode required a priori in SSA retrieval, the requirement in FMF retrieval is relatively lower.

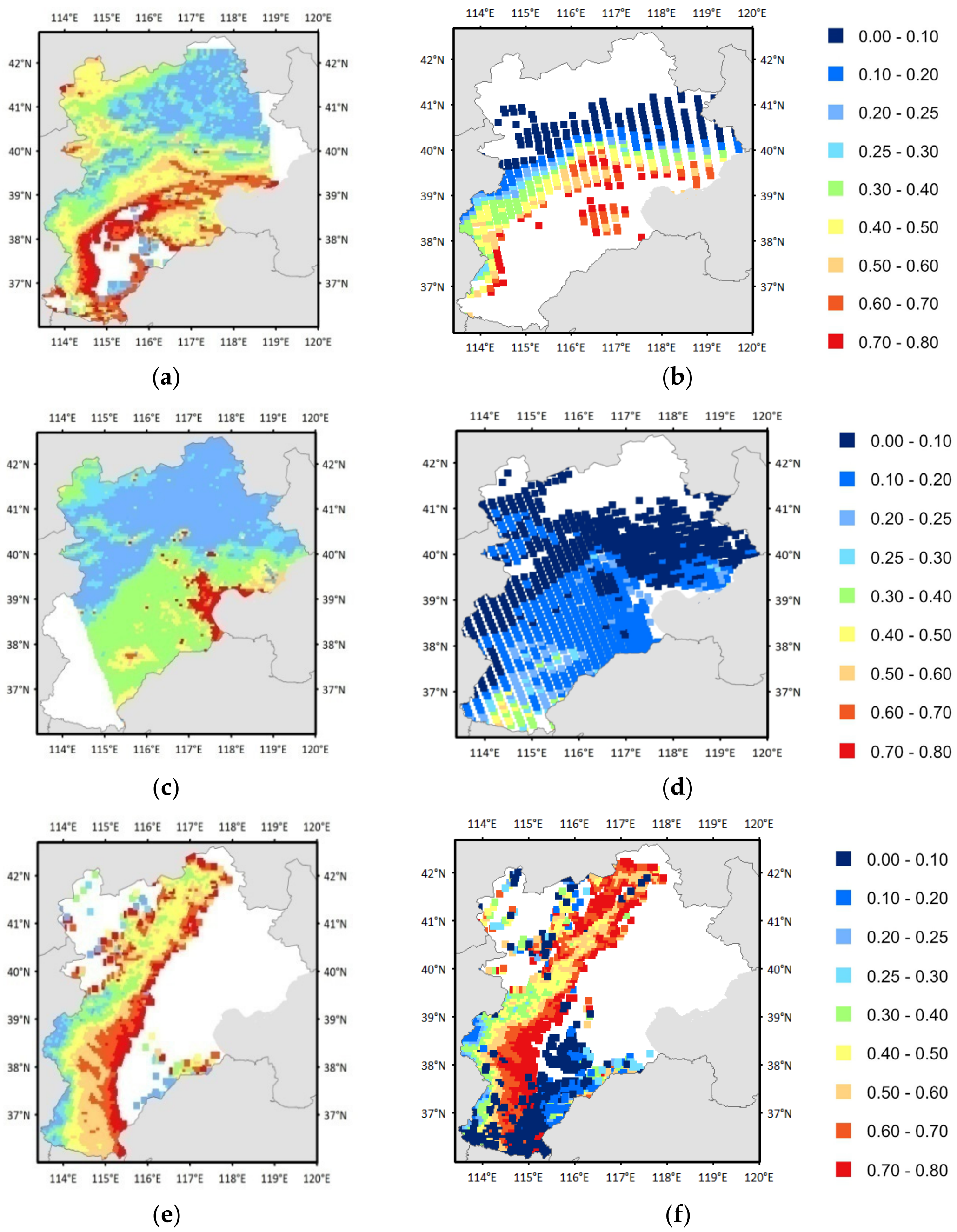

Figure 5. The AOD distribution of Jing-Jin-Ji area retrieved using PARASOL data for haze on 6 October 2009 (**a**), clear sky on 14 October 2009 (**c**), and dust on 20 March 2010 (**e**). The corresponding AOD distributions from MODIS for the same area and time period (**b**,**d**,**f**), respectively.

3.2. Case Studies Conducted over East China

Cases studies were carried out over east China for different aerosol scenes to evaluate the performance of the retrieval algorithm. Figure 2 shows the AOD distribution of the Jing-Jin-Ji area for haze, clear sky, and dusty weather, respectively. The corresponding AOD distributions of Aqua MODIS Dark Target products (c6) with a resolution of 10 km for the same area and time are also shown for comparison.

Figure 5a,b show a typical haze case in the Jing-Jin-Ji area, where high aerosol loadings are mainly centered in the southern part of the region as most industry factories are located there. The pixel-to-pixel comparison between our AOD retrievals and MODIS products over the Jing-Jin-Ji region yielded a correlation (R) of 0.895, a slope of 1.252, and an intercept of -0.105. This result shows that our AOD retrievals agree reasonably with MODIS products. The AOD values in the southeast of Jing-Jin-Ji are greater than 0.6, with most regions presenting values over 0.8. The mountain areas in the north and west parts of Jing-Jin-Ji always have much lower aerosol loadings, for which the AOD values mainly range between 0.1 and 0.3. For the clear sky case shown in Figure 5c,d, the average AOD of close to 0.4 in the south is obviously higher than that of 0.2 in the north. For the dusty case shown in Figure 5e,f, since the dust in this area is mostly contributed by the desert in the northwest of China, the dust particles that travel to the area are mostly blocked by the Yan Mountain and then deposited. That is why there is a clear high aerosol loading boundary with an AOD higher than 0.7 along the mountain. It can be seen from Figure 5 that the PARASOL and MODIS AOD retrievals show relatively similar distributions and magnitudes, indicating that the AOD retrievals with PARASOL are reasonable and can be used in different aerosol loading scenes. However, the results reported here are preliminary, and additional experimental data analysis is needed to improve the retrievals of the case studies.

4. Conclusions

An extended LUT aerosol retrieval algorithm based on surface reflectance angular shape invariance was applied to PARASOL measurements of total intensity and polarization to retrieve the optical properties of aerosols, which include the total AOD and the parameters related to the aerosols' microphysical properties, i.e., FMF and SSA. The spectral reflectance shape invariance principle was used to separate the TOA reflectance contribution from aerosol scattering and surface reflectance. The aerosol properties with Xangular values within the threshold can be regarded as preliminary aerosol retrievals. The preliminary aerosol results with similar Xangular indexes correspond to similar aerosol properties that can be distinguished using polarization measurements.

A comparison of the PARASOL AOD retrievals against the AOD measurements of different AERONET sites in China was conducted. The RMSEs were found to be smaller at urban sites like Beijing and Hefei, and this finding can be attributed to the better performance concerning the spectral reflectance shape invariance principle in urban areas and the easier separation of surface and aerosol scattering contributions. The linear regression slopes for nearly all the sites are larger than 0.7, except for those of the SACOL and Jingtai dust sites.

Case studies conducted over east China for different aerosol scenes were carried out to evaluate the performance of the retrieval algorithm. The AOD distribution of the Jing-Jin-Ji area for haze, dust, and clear sky were investigated. The simultaneous AOD products of MODIS (C6) for the same area were also given for comparison. The comparison of the AOD regional distribution showed that two AOD products have similar distributions.

The FMF validation results, namely, an RMSE of 0.23, a correlation coefficient of 0.57, and a bias of -0.01, show relatively high sensitivity in distinguishing the fine and coarse modes of particle contribution.

In the future, additional experimental data analyses will be carried out to improve the retrievals of the case studies. The algorithm will be further optimized and applied to other MAP satellites in orbit.

Author Contributions: Conceptualization, S.W.; methodology, S.W. and L.F.; software, L.F.; validation, L.F. and W.G.; formal analysis, S.W; investigation, W.G.; data curation, S.W.; writing—original draft preparation, S.W.; writing—review and editing, W.G. and L.F.; visualization, L.F. and S.W.; supervision, W.W. and S.T.; project administration, W.W; funding acquisition, W.W. All authors have read and agreed to the published version of the manuscript.

Funding: This research was funded by the National Natural Science Foundation of China (Grant No: 41975032) and the Key Project of the National Natural Science Foundation of China (Grant No: 42230109).

Data Availability Statement: The AERONET data used in this study are available via https://aeronet.gsfc.nasa.gov/ (accessed on 28 February 2019). The PARASOL L1B data were provided by the ICARE center. The used MODIS data are available from the Level-1 and Atmosphere Archive and Distribution System (LAADS) (https://ladsweb.modaps.eosdis.nasa.gov/search/) (lastly accessed on 25 August 2022).

Acknowledgments: We thank the ICARE center for providing the Level 1 and Level 2 datasets of PARASOL. We are also thankful to the AERONET team and PIs for maintaining the sites and sharing the data used in this study.

Conflicts of Interest: The authors declare no conflicts of interest. Li Fang is an employee of China Siwei Surveying and Mapping Technology Company. The company had no role in the design of the study; in the collection, analysis, or interpretation of data; in the writing of the manuscript, or in the decision to publish the articles. The paper reflects the views of the scientists and not the company.

References

1. Sano, I.; Mukai, S. Investigation of air pollution and regional climate change due to anthropogenic aerosols. In *Remote Sensing Technologies and Applications in Urban Environments*; SPIE: Bellingham, WA, USA, 2016; Volume 100080Z.
2. Kaufman, Y.J.; Boucher, O.; Tanré, D.; Chin, M.; Remer, L.A.; Takemura, T. Aerosol anthropogenic component estimated from satellite data. *Geophys. Res. Lett.* **2005**, *32*, 317–330. [CrossRef]
3. Degrendele, C.; Okonski, K.; Melymuk, L.; Landlová, L.; Kukučka, P.; Čupr, P.; Klánová, J. Size specific distribution of the atmospheric particulate PCDD/Fs, dl-PCBs and PAHs on a seasonal scale: Implications for cancer risks from inhalation. *Atmos. Environ.* **2014**, *98*, 410–416. [CrossRef]
4. Mishchenko, M.; Cairns, B.; Kopp, G.; Schueler, C.F.; Fafaul, B.; Hansen, J.; Hooker, J.; Itchkawich, T.; Maring, H.; Travis, L.D. Accurate monitoring of terrestrial aerosols and total solar irradiance: Introducing the Glory Mission. *Bull. Am. Meteorol. Soc.* **2007**, *88*, 677–691. [CrossRef]
5. Kokhanovsky, A.A. The modern aerosol retrieval algorithms based on the simultaneous measurements of the intensity and polarization of reflected solar light: A review. *Front. Environ. Sci.* **2015**, *3*, 4. [CrossRef]
6. Fougnie, B.; Bracco, G.; Lafrance, B.; Ruffel, C.; Hagolle, O.; Tinel, C. PARASOL in-flight calibration and performance. *Appl. Opt.* **2007**, *46*, 5435–5451. [CrossRef] [PubMed]
7. Wang, S.; Gong, W.; Fang, L.; Wang, W.; Zhang, P.; Lu, N.; Tang, S.; Zhang, X.; Hu, X.; Sun, X. Aerosol Retrieval over Land from the Directional Polarimetric Camera Aboard on GF-5. *Atmosphere* **2022**, *13*, 1884. [CrossRef]
8. Li, L.; Che, H.; Zhang, X.; Chen, C.; Chen, X.; Gui, K.; Liang, Y.; Wang, F.; Zhang, L.; Zhang, X.; et al. A satellite-measured view of aerosol component content and optical property in a haze-polluted case over North China Plain. *Atmos. Res.* **2022**, *266*, 105958. [CrossRef]
9. Jin, S.; Ma, Y.; Chen, C.; Dubovik, O.; Hong, J.; Liu, B.; Gong, W. Performance evaluation for retrieving aerosol optical depth from the Directional Polarimetric Camera (DPC) based on the GRASP algorithm. *Atmos. Meas. Tech.* **2022**, *15*, 4323–4337. [CrossRef]
10. Deuzé, J.L.; Bréon, F.M.; Devaux, C.; Goloub, P.; Herman, M.; Lafrance, B.; Maignan, F.; Marchand, A.; Nadal, F.; Perry, G.; et al. Remote sensing of aerosols over land surfaces from POLDER-ADEOS-1 polarized measurements. *J. Geophys. Res. Atmos.* **2001**, *106*, 4913–4926. [CrossRef]
11. Dubovik, O.; Herman, M.; Holdak, A.; Lapyonok, T.; Tanre, D.; Deuze, J.L.; Ducos, F.; Sinyuk, A.; Lopatin, A. Statistically optimized inversion algorithm for enhanced retrieval of aerosol properties from spectral multi-angle polarimetric satellite observations. *Atmos. Meas. Tech.* **2011**, *4*, 975–1018. [CrossRef]
12. Dubovik, O.; Fuertes, D.; Lytvynov, P.; Lopatin, A.; Lapyonok, T.; Doubovik, I.; Chen, C.; Torres, B.; Matar, C.; Federspiel, C.; et al. A Comprehensive Description of Multi-Term LSM for Applying Multiple a Priori Constraints in Problems of Atmospheric Remote Sensing: GRASP Algorithm, Concept, and Applications. *Front. Remote Sens.* **2021**, *2*, 23. [CrossRef]
13. Hasekamp, O.P.; Litvinov, P.; Butz, A. Aerosol properties over the ocean from PARASOL multiangle photopolarimetric measurements. *J. Geophys. Res. Atmos.* **2011**, *116*, D14204. [CrossRef]
14. Fu, G.; Hasekamp, O. Retrieval of aerosol microphysical and optical properties over land using a multimode approach. *Atmos. Meas. Tech.* **2018**, *11*, 6627–6650. [CrossRef]
15. Fang, L.; Hasekamp, O.; Fu, G.; Gong, W.; Wang, S.; Wang, W.; Han, Q.; Tang, S. Retrieval of Aerosol Optical Properties over Land Using an Optimized Retrieval Algorithm Based on the Directional Polarimetric Camera. *Remote Sens.* **2022**, *14*, 4571. [CrossRef]
16. Lu, S.; Landgraf, J.; Fu, G.L.; van Diedenhoven, B.; Wu, L.; Rusli, S.P.; Hasekamp, O.P. Simultaneous Retrieval of Trace Gases, Aerosols, and Cirrus Using RemoTAP—The Global Orbit Ensemble Study for the CO_2M Mission. *Front. Remote Sens.* **2022**, *3*, 914378. [CrossRef]
17. Xu, F.; Van Harten, G.; Diner, D.J.; Kalashnikova, O.V.; Seidel, F.C.; Bruegge, C.J.; Dubovik, O. Coupled retrieval of aerosol properties and land surface reflection using the Airborne Multiangle SpectroPolarimetric Imager. *J. Geophys. Res. Atmos.* **2017**, *122*, 7004–7026. [CrossRef]
18. Gao, M.; Franz, B.A.; Knobelspiesse, K.; Zhai, P.-W.; Martins, V.; Burton, S.; Cairns, B.; Ferrare, R.; Gales, J.; Hasekamp, O.; et al. Efficient multi-angle polarimetric inversion of aerosols and ocean color powered by a deep neural network forward model. *Atmos. Meas. Tech.* **2021**, *14*, 4083–4110. [CrossRef]

19. Wang, S.; Fang, L.; Zhang, X.; Wang, W. Retrieval of Aerosol Properties for Fine/Coarse Mode Aerosol Mixtures over Beijing from PARASOL Measurements. *Remote Sens.* **2015**, *7*, 9311–9324. [CrossRef]
20. Holben, B.N.; Smirnov, A.T.; Eck, T.F.; Slutsker, I.; Abuhassan, N.; Newcomb, W.W.; Schafer, J.S.; Chatenet, B.; Lavenu, F.; Kaufman, Y.J.; et al. An emerging ground-based aerosol climatology: Aerosol optical depth from AERONET. *J. Geophys. Res.* **2001**, *106*, 12067–12098. [CrossRef]
21. O'Neill, N.T.; Eck, T.F.; Smirnov, A.; Holben, B.N.; Thulasiraman, S. Spectral discrimination of coarse and fine mode optical depth. *J. Geophys. Res.* **2003**, *108*, 4559. [CrossRef]
22. Lenoble, J.; Herman, M.; Deuzé, J.L.; Lafrance, B.; Santer, R.; Tanré, D. A successive order of scattering code for solving the vector equation of transfer in the earth's atmosphere with aerosols. *J. Quant. Spect. Rad. Trans.* **2007**, *107*, 479–507. [CrossRef]
23. Parol, F.; Buriez, J.C.; Vanbauce, C.; Couvert, P.; Sèze, G.; Goloub, P.; Cheinet, S. First results of the POLDER "Earth Radiation Budget and Clouds" operational algorithm. *IEEE Trans. Geosci. Remote Sens.* **1999**, *37*, 1597–1612. [CrossRef]
24. Zeng, S.; Parol, F.; Riedi, J.; Cornet, C.; Thieuleux, F. Examination of POLDER/PARASOL and MODIS/Aqua Cloud Fractions and Properties Representativeness. *J. Clim.* **2011**, *24*, 4435–4450. [CrossRef]
25. Flowerdew, R.J.; Haigh, J.D. An approximation to improve accuracy in the derivation of surface reflectances from multi-look satellite radiometers. *Geophys. Res. Lett.* **1995**, *22*, 1693–1696. [CrossRef]
26. Kahn, R.A.; Gaitley, B.J.; Martonchik, J.V.; Diner, D.J.; Crean, K.A.; Holben, B. Multiangle Imaging Spectroradiometer (MISR) global aerosol optical depth validation based on 2 years of coincident Aerosol Robotic Network (AERONET) observations. *J. Geophys. Res.* **2005**, *110*, D10S04. [CrossRef]
27. Hulst, H.C.; van de Hulst, H.C. *Light Scattering by Small Particles*; Courier Corporation: North Chelmsford, MA, USA, 1981.
28. Dubovik, O.; Sinyuk, A.; Lapyonok, T.; Holben, B.N.; Mishchenko, M.; Yang, P.; Eck, T.F.; Volten, H.; Munoz, O.; Veihelmann, B.; et al. Application of spheroid models to account for aerosol particle nonsphericity in remote sensing of desert dust. *J. Geophys. Res. Atmos.* **2006**, *111*, D11. [CrossRef]
29. Nadal, F.; Bréon, F.M. Parameterization of surface polarized reflectance derived from POLDER spaceborne measurements. *IEEE Trans. Geosci. Remote* **1999**, *37*, 1709–1718. [CrossRef]
30. Smirnov, A.; Holben, B.N.; Eck, T.F.; Dubovik, O.; Slutsker, I. Cloud-Screening and Quality Control Algorithms for the AERONET Database. *Remote Sens. Environ.* **2000**, *73*, 337–349. [CrossRef]
31. Dubovik, O.; King, M.D. A flexible inversion algorithm for retrieval of aerosol optical properties from Sun and sky radiance measurements. *J. Geophys. Res. Atmos.* **2000**, *105*, 20673–20696. [CrossRef]
32. Chen, C.; Dubovik, O.; Fuertes, D.; Litvinov, P.; Lapyonok, T.; Lopatin, A.; Ducos, F.; Derimian, Y.; Herman, M.; Federspiel, C.; et al. Validation of GRASP algorithm product from POLDER/PARASOL data and assessment of multi-angular polarimetry potential for aerosol monitoring. *Earth Syst. Sci. Data* **2020**, *12*, 3573–3620. [CrossRef]